# DESICCATION CRACKING DETECTION USING 2-D AND 3-D ELECTRICAL RESISTIVITY TOMOGRAPHY: VALIDATION ON A FLOOD EMBANKMENT.

Gareth Jones[a], Philippe Sentenac[a], Marcin Zielinski[a,b]

**AFFILIATIONS:**

[a] Department of Civil and Environmental Engineering, University of Strathclyde, Glasgow, UK

[b] Zachry Department of Civil Engineering, Texas A&M University, College Station, US

**KEY WORDS:** Embankments, Detection, Desiccation, Cracks, Electrical Resistivity Tomography, Modelling

**CORRESPONDING AUTHOR:**

Gareth Jones

University of Strathclyde

Department of Civil and Environmental Engineering

James Weir Building

75 Montrose Street

G1 1XJ, Glasgow, UK

email: gareth.jones@strath.ac.uk

Phone: +44 (0)141.548.4751

**Highlights**

- ERT analysis of desiccation cracks in flood embankment during different seasons.
- Forward modelling of small and large fissuring networks.
- Validation of 2-D and 3-D miniature arrays on fissured flood embankment.
- Evaluation of standard ERT arrays on large section of flood embankment.
- Validation of field result with forward modelling.

## Abstract

Desiccation cracks forming in earthen structures are a known source of engineering concern. In particular such fissures forming in flood embankments can affect their stability leading to failure when overtopped. These and other problems related to safety have raised the importance of using efficient and reliable tools, especially when relatively fast, non-invasive and extensive investigations are required. Geophysical techniques, such as Electrical Resistivity Tomography (ERT), allow for accurate assessment and monitoring of shallow depths within engineering structures.

The presented study examines the use of miniature and field scale ERT on a fissured flood embankment near Hull, UK. Two separate sections were surveyed in summer and winter using both 2-D and 3-D configurations, allowing seasonal evaluation of embankment condition.

The field results were validated through forward modelling, with different fissure configurations and the effect of topography. The results show that the resolution of the cracks increased with smaller electrode spacing. It was found that ERT can be used on a larger scale to detect zones of fissuring with fissured networks being displayed. The ability to detect cracks was diminished when surveying in winter with cracks reducing in size due to seasonal swelling of the soil. The resistivity models obtained showed anomalies with far lower resistivity than those obtained in summer.

The study showed that miniature surveys could be used to examine small sections in detail allowing imaging for horizontal subsurface fissures. The larger scale surveys provided important spatial information allowing the distribution of fissures on the embankment to be made.

The study recommends that geophysical surveying of flood defences should be used as a routine assessment tool to detect desiccation cracks within the embankment, and that these surveys should be completed in the summer, where cracks are most prominent.

# 1 Introduction

In the UK more than 34,000 km of flood embankments protect homes and vital infrastructure along its coast and estuaries. With potential increase in sea levels estimated to be around 0.5m or more (van Vuren et al., 2011; Pardaens et al., 2011) as a result of global climate change, the strength and integrity of such flood defences are expected to be placed under increased scrutiny. When coupled with the predicted increase in precipitation (Met Office, 2011a) the importance of maintenance and inspection of flood defences is of increasing public importance in the UK. Recent extreme weather in winter 2013 has pushed the British Government to announce £140M of new funding for repairing and improving flood defences. These events have reinforced the need for effective flood mitigation and have brought the issue to the forefront of public debate, further emphasising the need for regular maintenance and assessment of existing flood embankments.

Currently flood embankments are only assessed through visual surveying, requiring the surveyor to walk the entire length of the structure to observe any possible weaknesses. The presence of defects such as desiccation cracks can be obscured by dense vegetation and as a result surveys are generally taken during the winter months when vegetation is lighter. Despite this, vegetation can still be heavy enough to impede the visual survey particularly on the landward side which is rarely maintained. The severity of the cracks inside the structure can be underestimated due to seasonal swelling of the soil during wetter months. In addition to visual surveys, only destructive techniques, such as sampling and trenching can be used to detect fissuring in depth. Hence, new techniques are needed which would allow non-invasive detection and characterisation of cracking in the near surface. In this study, non-destructive Electrical Resistivity Tomography (ERT) is proposed as a tool to detect the extent of desiccation in earthen structures. The use of miniature, 2-D and 3-D ERT arrays previously tested on laboratory models (Sentenac and Zielinski, 2009; Jones et al., 2012), was validated in situ on a desiccated flood embankment and compared with results obtained

from forward modelling. The use of field scale ERT was also investigated and validated through forward modelling. The results from different seasonal surveys on a desiccated embankment were compared and discussed.

## 1.1 Cracking due to desiccation

Desiccation due to moisture loss results in shrinkage of a soil mass. When shrinkage is restrained, as in massive structures such as flood embankments, cracks form due to build-up of internal stresses (Shin and Santamarina, 2011). With extended periods of desiccation, cracks can grow to form interconnected networks, providing a pathway for fluid flow (Sanchez et al., 2013). In flood embankments, such networks of fissures can result in failure during overtopping (Cooling and Marsland, 1954; Marsland and Cooling, 1958). Desiccation cracks separate the soil into polygonal blocks at the surface while continuous shrinkage can result in a shear plane beneath the surface of the soil (Konrad and Ayad, 1997; Style et al., 2010), resulting in the separation of the top layer of soil from the remainder of the structure (Figure 1). Such cracking is of concern in several engineering and agricultural applications; e.g. compacted clay landfill liners (Kleppe and Olson, 1985; Omidi et al., 1996; Southen and Rowe, 2005; Albright et al., 2006) and irrigation quality (Liu et al., 2003; Janssen et al., 2010). In general terms the problems relate to the creation of direct flow paths through the material, due to the increased permeability as the result of interconnection between adjacent fissures.

### 1.1.1 Embankment failure due to desiccation cracks

Desiccation in flood embankments is a global process and is likely to affect the embankment body including the crest and both slopes. Failure can be induced during overtopping where water can infiltrate via large surface cracks and flow through the fissured network (Marsland, 1957). This flow can result in internal erosion of the fissured pathways, leading to instability of the embankment slopes and leading ultimately to breach (Cooling & Marsland, 1954). The failure method resulting in breach in engineering terms, can be considered as a rigid block

rotating away from the embankment (Utili, 2012), and the landward side of an embankment may be considered to have the highest risk of failure.

In some cases seepage through the fissures can be observed without water reaching the crest of the embankment (Zielinski 2009). In such case, the effective height of protection is reduced to the height of the intact part of the soil.

Research conducted by Cooling and Marsland (1954) and Marsland (1968) after the 1953 North Sea floods revealed a large number of wide cracks (≈10cm) penetrating flood defences to a depth of about 1.5m. A later study carried out by Dyer et al. (2009) on the disused Thorngumbald embankment, near Hull (UK), discovered a specific character of cracking, forming a relatively shallow (about 60cm) interconnected network with both, vertical and horizontal fissures present. Another example from the same study shows an individual crack extending to a depth of 1m.

From these studies it can be seen that the nature of soil fissuring can vary from case to case, and that gathering such information about its extent within the structure is impossible without destructive trenching into the embankment body. This or even less invasive tube sampling, if necessary, has to be limited to a small area since the structure cannot be affected; hence the investigation is very limited. Thus, some advanced and non-invasive techniques are needed for high quality sub-surface assessments, particularly in cases where the fissured structure is at risk.

## 1.2 Electrical Resistivity Tomography

Electrical Resistivity Tomography (ERT) is a frequently used Geophysical technique that allows the electrical properties of a section of ground to be determined by measuring the drop in potential occurring due to an applied electrical current (Reynolds 1997). Such a method has been used successfully in the laboratory for the detection and monitoring of fissures in clayey soil (Samouëlian et al., 2003; Samouëlian et al., 2004, Sentenac and

Zielinski, 2009; Jones et al., 2012). An additional advantage for the use of ERT is its potential use in remote monitoring (La Breque et al., 2004; Rucker et al., 2009; Sjödahl et al., 2008; Kuras et al., 2009; Wilkinson et al., 2010; Wilkinson et al., 2011). Such monitoring is advantageous as it allows the site to be monitored without the presence of a surveying team, with data being sent automatically for processing. When doing long-term monitoring with ERT, temperature variations should be accounted for (Keller and Frischknecht 1966, Abu-Hassanein et al., 1996; Johansson and Dahlin, 1996; Zha et al., 2010). Previous studies have shown that there is a 2% rise in resistivity with each 1°C drop, relative to a reference temperature (Sjödahl et al., 2008; Ling et al., 2013; Pellicer et al., 2012).

Since the temperature changes within an estuarine flood embankment are usually complex, and available atmospheric data was restricted to air temperature and precipitation only; it was not possible to apply these methods to predict the temperature within the structure. In this study it was assumed that changes in measured apparent resistivity between different periods would be due to seasonal changes in moisture which are not greatly influenced by seasonal temperature changes.

### 1.2.1 ERT and cracking

When implementing ERT in fissured soil, it can be considered that single cracks act as barriers impeding the flow of charged particles (positive cations and negative anions), resulting in an apparent drop in potential relative to that observed for the surrounding intact soil (Rhoades et al., 1989). These cracks can be considered to be an anomaly of virtually infinite resistivity given that it can be seen to be an air gap, though the true resistivity of cracks is lower as the measurement includes some part of the surrounding intact soil. In Jones et al. (2012) some consideration was given to the possible range of resistivity values that could be attributed to a fissure forming in clay. Based on observations in literature (Reynolds, 1997 and Loke, 2014) it was assumed that a resolved anomaly with values of 100 ohm-m or more could be considered to be a fissure given that this was the upper limit

observed for intact clay. This range was verified in the laboratory (Jones et al., 2012) using a small electrode spacing of 4.5cm.

In the same study, both Schlumberger and Dipole-Dipole arrays were used individually and in a combined inversion to examine the effectiveness of each array for the visualisation of fissures in the subsurface. It was found that the combined inversion provided the most accurate image of subsurface fissuring. The study recommended that the Schlumberger array should be used for field measurements, due to its relatively fast survey times, and strong imaging of subsurface fissures. Sentenac and Zielinski (2009) also used the Schlumberger array to image fissures forming in 2-D. The study showed that the fissures could be resolved and their evolution tracked. Earlier studies (Samouëlian et al., 2003) used single 2-D Wenner array to resolve fissures created artificially on a clay block and later using the square arrays to track the growth of fissures in 3-D (Samouëlian et al., 2004).

A field study by Sentenac et al. (2012) presented a possible approach for detecting fissured areas in flood embankments by using complementary Electromagnetic and low resolution resistivity surveys. The concept was based on relating high resistivity responses to potentially fissured zones and comparing them with the Electromagnetic surveys carried out over the same sections of two different embankments and during both summer and winter seasons. The study also showed the ability of the ERT in exploring desiccated and fissured zones in the cross-section of an embankment.

The past research presented above shows that cracks forming in clay can be monitored and detected in 2-D and 3-D under laboratory conditions using high resolution miniature ERT arrays. For the field, areas of potential fissuring can be detected through visualisation of high resistivity zones. The use of miniature and field ERT for detecting and characterising individual cracks has not yet been verified in situ. This study uses high resolution methods developed in the laboratory and applies them to a fissured flood embankment. The

characterisation of fissuring in 2-D and 3-D using both configurations was compared with computational forward models.

# 2 Forward modelling

To improve the reliability and help the interpretation of field results, an extensive modelling was carried out. The produced models were designed to represent idealised fissured networks with small width (cm scale) cracks, such as those previously found on the surveyed embankment (Dyer et al., 2009). The modelling of several small scale models represented the stages in the fissuring process, as well as complex interconnected fissuring patterns with horizontal subsurface fissuring. Additionally, large scale models were created with extended fissured sections, in order to investigate the effect of large scale arrays (e.g. electrode spacing of 0.5 to 1m) on relatively small targets (10 cm wide cracks). Each model was created to investigate the potential response to a survey conducted over a complex fissuring network in the near surface.

Figure 2a shows the geometry of the fissuring pattern used for the input to the small scale forward model with the cracks modelled as resistivity elements of 1000 ohm-m and contrasted background of 20 ohm-m for the surrounding, intact soil. Modelling was completed using the RES3DMOD forward modelling software on the High Performance Computer (University of Strathclyde) which allowed large datasets to be modelled without applying assumptions about scaling. The cracks could be modelled as small individual cells of 10cm on a large scale model, rather than assuming that the apparent resistivity would reduce with increasing electrode spacing. Such an effect could be investigated directly from the models themselves. The small scale models were computed using the Finite Element Method, while the large scale models required the Finite Difference Method.

## 2.1 Small scale

The scale of the smaller survey is analogous to the 2-D miniature slope surveys discussed later in Section 4.1.2 of the paper. The cracks were modelled as elements of 10 cm, which

for this model is the electrode spacing maintained for the inversions, and is also the size of the larger fissures observed in the field.

Presented in Figure 3 are the results from the 2-D inversions of the small scale fissures, located at 1.5m from the edge of the model, as indicated in Figure 2a with fissure depths of 0.5 and 1m. For consistency with laboratory measurements in Jones et al. (2012) and the field results presented in Section 3 and 4, the models are presented here for the Schlumberger method. As can be seen in Figure 3a, the inversion has resolved both vertical (starting from the surface) and horizontal fissures at a depth of 0.3m. The addition of noise to the data set has resulted in a loss of resolution for the horizontal fissure. The horizontal fissure is still distinguishable from the background resistivity in this idealised setup, even at relatively high noise levels of 40%. The vertical cracks leading from the surface are also distinguishable down to 0.2m where the horizontal fissures are resolved. Vertical fissuring is not resolved below this point, though this is likely to be due in part to the geometry of the survey as the fissures lie out with the measurable zone. In the presented results, clear contrast can be seen between the cracked and intact soil, with fissures visible as high resistivity anomalies of 100 ohm-m or above, relative to the background, intact soil with resistivity of around 20 ohm-m, close to the input value used for the soil. The addition of noise blurs the resolved anomalies and lower resistivities (40 to 50 ohm-m) can be seen to represent the horizontal fissures (Figure 3b), with high levels of noise resulting in some features being obscured entirely (Figure 3c)

## 2.2 Large scale survey

In addition to the miniature scale modelling, another analysis was completed on a field scale to investigate the effect of larger electrode spacing on the resolution of small scale cracks. The input model was based on the fissuring pattern on the miniature model shown in Figure 2a with cracks of 10cm width. The fissuring here formed a more extensive network as shown in Figure 2b and c. The model itself had dimensions of 14m in the x-direction and 6m in the y-direction, with fissures modelled on the first 10m in the x-direction only. This ensured that

any anomalous effect due to the addition of noise added to the data set could be observed on the non-fissured section. Once the forward modelling was completed, the data was extracted with electrode spacing of 0.5 and 1m. Inversions were completed with these data sets in both 3-D and 2-D in the x-direction only. 2-D inversions were run on sections separated by 1m in the y-direction.

Models are shown with fissures at 1m depth using Schlumberger array and with a random noise of 0%, 20% and 40% applied to the analysis. Figure 4 shows the surface of the resistivity models from the 3-D inversions, for electrode spacing of 0.5 and 1m and with the true fissure location superimposed. The initial model with 0.5m electrode spacing before the noise was added shows a well resolved surface layer, with the pattern of high resistivity closely matching the input fissure positions. It can be seen in Figure 4c and Figure 4f, that the addition of noise introduces some discrete anomalies within the non-fissured layer particularly at high noise levels.

Vertical cross sections taken at 2 and 3m as indicated in Figure 2b, and c show the fissuring for 3-D inversions with 0.5m and 1m electrode spacing (Figure 5 and 6). The corresponding 2-D inversions with 1m electrode spacing are shown in Figure 7. The vertical sections show that the fissuring is well represented by the resistivity model with the electrode spacing of 0.5m. High resistivity anomalies can be seen to extend to 1m depth matching the input fissuring depth used in the forward model. The cracks themselves are resolved with high resistivity relative to the background values of 20 ohm-m, and can be plotted on the same scale as the miniature surveys shown in Figure 3. The values of resistivity reduce as the fissuring depth approaches 1m, but the cracks are still distinguishable from the background intact soil, albeit with low resistivity values of 30 ohm-m (Figure 5).

The model with 1m electrode spacing shows a similar trend to the one with lower resolution and reduced values of resistivity. The fissured, zone is clearly distinguishable from the intact section where no noise is added to the model and the fissures have resistivity of around 40 to 100 ohm-m compared with background resistivity of 20 ohm-m. The addition of noise shows the same effect as the 0.5m spacing model, with some high resistivity anomalies

appearing in the intact zone (Figure 6b to 6f). The 2-D inversion shows a similar set of results, though the data appears to be more affected by the noise than the 3-D inversions (Figure 7c and Figure 7f). This is understandable as the 3-D inversion is constrained by data from parallel data sets. This is reflected in a more uniform subsurface and a lower absolute error for the 3-D model in comparison to the 2-D. In general, the two inversion models produced the same image of the subsurface, with high resistivity zones corresponding to fissure locations.

The vertical cross sections show a similar trend to those obtained from the 0.5m electrode spacing model and the high resistivity anomalies have been resolved to 1m, in agreement with the input model.

As expected, the image resolution of the fissures and complex structures (e.g. horizontal fissures) reduces with increasing electrode spacing. The reduction of the vertical resolution of the fissures is not significant and it is still possible to obtain a reasonable reconstruction of the resistivity model with electrode spacing of 1m and high noise levels of 40%.

### 2.2.1 Non-inline crack effect

The forward models show the effect of high resistivity anomalies running adjacent to the survey lines. This is particularly true for the models with 1m electrode spacing, shown along the Y-axis (Figure 6 and Figures 7d, e and f). In this setting the electrodes are 0.1m away from the crack and the anomalies are resolved as a zone of high resistivity (approximately 40 to 50 ohm-m). These values are close to input parameters for the fissures. Nevertheless they could be misinterpreted as zones of fissuring crossing the survey line, particularly for the 2-D inversion where a surface view such as in Figure 4 is not available. This effect is less pronounced for smaller electrode spacings making the issue limited to large scale surveys. This however can be considered to be advantageous for larger scale surveys in low resolution reconnaissance of the condition of the structure.

## 2.3 Effect of topography

In this study the effect of both inline and non-inline topography on the resistivity models was investigated using forward modelling. 3-D models with uniform resistivity values were created. The models were then compared with the input, flat model (model with no topography) with resistivity of 20 ohm-m, allowing the areas most affected by topography to be observed.

A resistivity ratio defined as the resistivity of model with topography relative to the flat model was used to analyse the effects of topography on both apparent resistivity and inverted resistivity models. The models are based on the geometry of Thorngumbald embankment, with crests of 3m width and slopes modelled with 30º relative to the horizontal.

### 2.3.1 Non-inline topography

Non-inline topography was analysed by creating a coarse model, with 1m electrode spacing in the x-direction and 0.5m in the y-direction. The input model consisted of 29 electrodes in the x-direction (across the embankment) and 101 in the y-direction, with a crest of 3m width, similar to that found on the Thorngumbald embankment. An apparent resistivity model was obtained with data in the y-direction for the central line of electrodes. Analysis of the variation in resistivity indicated that surveys placed at the centre of the embankment were relatively unaffected by the topography. A maximum apparent resistivity ratio of 1.13 was found at a depth of around 7.1m below the surface of the model with a minimum ratio of 0.98 at the top layer.

### 2.3.2 Inline topography

The input model used to test inline topography consisted of electrode spacing of 0.5m in both the x and y-directions, with 33 electrodes modelled in the x-direction and 13 in the y-direction. In order to obtain a cross section of the embankment with parallel lines the data were modelled only in the x-direction. The output data from the forward model was then inverted with the topography included, and compared to the flat model. The apparent

resistivity model shown in Figure 8a and the resistivity model obtained in Figure 8b are symmetrical and as a result only a single slope (e.g. half model) is used in the analysis.

The results show that there is a small reduction in apparent resistivity at the bottom of the model while the resistivity increase can be noticed towards the crest (Figure 8a). The apparent and inverted results for the top layer where cracking is most likely to be detected are plotted in Figure 8c. The graph shows that the apparent resistivity ratio is less than unity at a single point, indicating that the resistivity is slightly elevated for the majority of the embankment slope and crest. A similar pattern can be seen for the inverted model with the entire top layer having an elevated resistivity relative to the ideal flat model. The highest resistivity contrast can be seen close to the crest with maximum resistivity ratios of 1.2.

The above study shows that the embankment topography will have an effect on the measured and inverted resistivity. However, for the resistivity ranges obtained in the study this increase is small enough not to affect the analysis of the results. In particular the top layer of the model will have slightly higher resistivity (approximately 10%) than the same section on a model with no topography. This increase in resistivity is greatest at the edge between the slopes and the crest (approximately 20%).

Figure 8d shows the histograms of the resistivity ratios obtained from the inversion models and apparent resistivity shown in Figure 8. The histogram shows that the majority of the data, 53.6% and 54.6% respectively, increased relative to the flat model while 41.1% and 39.7% have a reduced resistivity. Data that showed no increase or reduction in value accounted for 5.2% and 5.7%. The results indicate that the model is well balanced between increased and reduced resistivity levels. More importantly the variation of resistivity is generally small (less than 10%), as found with the non-inline model.

For the inverted model, it can be considered that when topography is accounted for, the inversion returns a well constrained model of the subsurface.

# 3 Field study – Thorngumbald, UK

Field surveys were completed on a naturally desiccated flood embankment (Paull Holme Strays, Humber estuary, England) known as the Thorngumbald embankment. The embankment was constructed in 2003 using locally sourced alluvial clays. Particle size distribution tests carried out on the soil sample reveal the following fractions: 35% sand, 48% silt, 17% clay, and with 9% of organic matter. The Atterberg's limits were found to be: liquid limit (LL) — 42%; plastic limit — 24%; and shrinkage limit — 15%. According to the British Standard 1377-2 (BSI, 1996), investigated soil can be described as silty clay of intermediate plasticity. The soil particle density is around 2.63 $Mg/m^3$. The X-ray diffraction analysis carried out on the powdered material shows the presence of quartz as a main mineral. More precise measurements carried out on the 425 μm fraction highlighted the presence of calcite, dolomite, illite and kaolinite. The activity of the soil, was found to be A=1.05, which is considered to be normal.

The first extensive fissuring on the Thorngumbald embankment was observed as early as 2006 (Dyer et al., 2009). A plan of the site is shown in Figure 9 with the locations of the surveys. The air temperature obtained from the weather station located at Keyingham 6.5km east from the surveyed embankment varied through the years with the recorded minimum temperature of 2°C in March 2011 and maximum of 19°C in June 2011 (Met Office, 2011b).

All surveys presented in the following sections were carried out to validate the procedures used by Jones et al. (2012) on the laboratory scale 2-D and 3-D models. The sensitivity of large scale surveys to the fissured networks was also investigated.

## 3.1 Surveys

### 3.1.1 Resistivity equipment

The earth metre ARES unit from GF instruments (Brno, Czech Republic) was used to measure the resistivity. As explained before the Schlumberger N6 array was chosen in the device. This array configuration has previously been successful in the laboratory for the

imaging of cracks (Sentenac and Zielinski, 2009; Jones et al., 2012). For the small scale surveys, 2mm diameter copper electrodes (Sentenac and Zielinski, 2009) were used, while the large scale 'standard' surveys were conducted with 1cm diameter stainless steel electrodes. During the large surveys, commercially available cable reels with 24 ports and maximum spacing of 2m were used, while custom built miniature cable was designed in conjunction with the miniature copper electrodes.

### 3.1.2 Visual survey

Localised visual surveys were also completed on the surveyed sections before each ERT survey in order to assess the current state of the embankment. The main observations were that cracks were found to be wider and more pronounced in the summer than in the winter, and that vegetation was denser in the summer. The larger cracks observed in the summer is a result of high shrinkage in the soil mass caused by excessive water loss during prolonged dry seasons (Zielinski et al., 2011). The largest fissures were observed in September 2010 and were found to be approximately 10cm wide at the surface forming polygonal blocks on the embankment outward slope (estuary side). In March 2011, during the winter months (Figure 10), fissures were found to be less pronounced having widths of about 2cm. Vegetation was dense in both the September 2010 and the June 2011 surveys, however some mowing of the grass on the crest and outward slope in August 2010 made cracks easier to identify in September. The landward slope (slope facing in-land) was always overgrown and fissuring was difficult to observe, even in March 2011 when the grass was visibly shorter.

### 3.1.3 Geophysical survey

In total, four site visits were made to Thorngumbald, with initial visual surveys completed in June 2010. This allowed for careful and detailed assessment of the entire length of embankment. The presence of cracks was confirmed and the locations for future 2-D and 3-D ERT surveys were selected. A survey in September 2010 produced extensive surveying of

the embankment crest covering 1.5km on both Sections 1 and 2 of the site as indicated in Figure 9, taking two days to complete. Electrode spacings of 2m were used throughout the crest survey allowing a large section to be measured in each reading. A cross embankment survey was also carried out on Section 1 with 0.5m electrode spacing. The aim was to examine whether differences between the embankment crest and the two slopes could be observed and individual cracks could be identified. More details can be found elsewhere (Sentenac et al. 2012). Additional surveys were also completed on the estuary slope with large sections surveyed with 1m electrode spacing, and overlapping high resolution miniature surveys (10cm and 5cm electrode spacing). It was observed that the survey with 5cm spacing contained a large number of negative data points, and data producing RMS errors in excess of 100% in the inversion. The negative data is thought to be the result of the high contrast between the intact soil and the fissures, close to the electrodes as discussed in Cho et al. (2002) and Wilkinson et al. (2008).

The first 3-D survey was completed in March 2011 and was located at Section 1 of the embankment. In total 3 surveys were completed over 2 days using the cross diagonal method. A large survey was taken across the embankment with 1m electrode spacing, in a 12 by 4 electrode grid. For this trial, measurements were taken over discrete sections as described in Jones et al. (2012). It was considered that continuous measurement would have increased the survey time with only a small gain in extra data with the available equipment. Additionally the miniature arrays used in the survey utilising 0.2m spacing proved difficult to reposition. It was acknowledged that rolling surveys would have produced a slightly improved model of the embankment, though the authors feel that the discrete measurements provide sufficient coverage to prove the applicability of the concept allowing analysis of the fissuring. A similar approach was successfully used by Jones et al. (2012).

In total an area of 11m by 15m was surveyed comprising 4 discrete sections. Overlapping surveys with 0.2 and 0.5m electrode spacing were taken in order to obtain higher resolution measurements of the visually observed fissuring. The main survey line was rotated by 90

degrees relative to the larger initial survey, and orientating the measurements along the length of the embankment. As before each survey was divided into grids consisting of 12 by 4 electrodes, with maximum survey lengths of 5.5m and 2.2m achieved. Additionally, two 2-D surveys were carried out on the crest using the same setup as during the September survey and covering 94m on Section 2 and 48m on Section 1 in Figure 9.

The final field trip completed in June 2011, produced a single large 3-D measurement using cross embankment parallel lines. In total the survey took one day to produce with 14 lines of data acquired, each using 24 electrodes. Electrode spacing of 0.5m was applied, with the survey lines separated by 1m, creating an overall surveyed area of 11.5m by 14m.

It was found from the standard surveys that the contact resistance between the soil and the electrodes was the highest in June with values as high as 500 ohm obtained with the standard size electrodes inserted approximately 10 to 15cm into the soil. The lowest contact resistances were observed in March with average values as low as 80 ohm recorded which conforms with the visual observation of high soil saturation of the embankment in March 2011. As expected, the miniature electrodes produced higher resistances due to the reduced contact area with the soil. The resistance values of 2000 ohm were observed in September 2010, while in March 2011 the miniature electrodes produced lower contact resistances with average values of 500 ohm.

### 3.1.4 Data inversion

**2-D data**

The 2-D data was inverted using RES2DINV Software (Loke and Barker 1996). Inversion was completed using parameters similar to those discussed in Jones et al (2012) using robust or L1 norm constraint to ensure high contrast between the fissures and the intact soil. Additionally, model blocks of half the electrode spacing were used with a complete Gauss-Newton iteration, with the model discretized using the finite element method with 4 nodes between each adjacent model cell. Iterations were limited to 20 as a default, though each

data set converged to 5% in less than 15 cycles. Some additional post processing was required to ensure that resistivity values resulting in errors of 75% or greater were removed from the data set and the inversion repeated.

***3-D data***

The resistivity files for each of the individual survey sections were combined into a single file and topography was added, based on the measured embankment geometry. The data was inverted using RES3DINV. The model constraints were the same as applied for the larger 2-D model except that the incomplete Gauss-Newton iteration was used to reduce the inversion time for the complex 3-D sections. Additionally the models were expanded outside the survey area by half the electrode spacing in each case in an attempt to improve the resolution of fissures at the edge of the model, as discussed in Jones et al. (2012).

# 4 Results and Discussion

## 4.1 2-D Survey

### 4.1.1 Crest surveys

Figure 11 presents the resistivity sections obtained from the surveys taken along the crest of the embankment. The profiles from September 2010 (Figure 11a to 11c) show a top layer with elevated resistivity ranging from 20 to 40 ohm-m, which is underlain by lower resistivity zone (5 to 15 ohm-m). These resistivity sections indicate that desiccation affects the top 1m of the embankment structure, with the underlying soil remaining intact. This would appear to be a reasonable assessment considering the time of year and the observed embankment condition with fissures visible on slopes and crest. No signs of individual cracks were observed from the obtained resistivity sections, which was due to the large electrode spacing (2m) used in this survey.

It is also consistent with the embankment condition at the time of the survey, where no significant cracking was found on the crest. In comparison, the 2-D survey obtained in March

2011 (Figure 11d), shows a more homogeneous model with higher resistivity values than those obtained from the previous site visit in September 2010. The desiccated top layer observed at that time (Figure 11a to 11c) was not as apparent as the level of soil saturation was higher in the winter months. Smaller cracks on the embankment slopes were observed and lower contact resistance was measured between electrodes and the soil. The two surveys obtained in March show the effect of higher embankment saturation. This is particularly true for winter months when the precipitation exceeds evapotranspiration (Smethurst, 2006). The lower resistivity measured in Section 1 may also be attributed to direct exposure to the water from the Humber River (located in front of the breached section of the original embankment as shown in Figure 9).

It can be seen in Figure 10 that the amount of precipitation in February and March 2011, was lower than the one in August and September 2010, which would result in a generally drier embankment. This would account for the higher overall resistivity observed in Section 2 of the embankment in the March 2011 survey.

#### 4.1.2 Slope surveys

Surveys completed on the embankment outward slope show the effect of increased resolution with reduced electrode spacing. Figure 12, shows the slope surveys obtained using electrode spacing of 1m with the positions of overlapping, miniature surveys indicated. An area of higher resistivity (20 to 40 ohm-m) can be observed on both profiles, with low resistivity (0 to 15 ohm-m). Patches of higher resistivity (40 to 90 ohm-m) can also be seen close to the surface of the soil. These results are consistent with the large scale 2-D forward modelling as shown in Figure 12. Individual cracks could not be resolved due to the low resolution obtained with large array configuration. In contrast the miniature surveys obtained with the electrode spacing of 10cm are shown in Figure 13 accompanied with photographs of the embankment surface. The positions of the high resistivity anomalies are consistent with the visual observation of the embankment surface presented in Figure 13 and reveal the

vertical and horizontal fissures. These subsurface anomalies are similar to those resolved for the 2-D inversion of the forward model (Figure 3), indicating that such anomalies may be the result of subsurface fissures as observed by Dyer et al. (2009). The depth of the connecting subsurface horizontal anomaly falls between 0.1m and 0.2m, which is also consistent with those exposed on the original Thorngumbald embankment (Dyer et al., 2009).

Based on the small scale modelling shown in Figure 3, it can be seen that the fissuring below a depth of 0.5m is difficult to resolve in the presence of relatively high noise. The same effect can be noticed from the field data. However the results obtained down to a depth of 0.5m, are consistent for both the forward models and the field resistivity models.

The resistivity models revealed that the majority of cracks extend to shallow depths of 0.2m for both the surveys at Sections 1 and 2. Larger fissures were resolved to depths of 0.5m on Section 1 (fissures B and E on Figure 13a). Higher zones of resistivity (50 to 70 ohm m) can be seen at depths of 0.5 to 1m (Figure 13b). As discussed before, these areas may represent fissures with low resolution.

A better estimation of the true extent of fissuring was obtained from the large scale surveys (Figure 12). The results are in agreement with the forward model inverted in 2-D, with fissures of 1m depth. Figure 12a and Figure 12b shows the different depths of high resistivity values. It can be seen that Section 1 exhibits a shallower (e.g. 0.5m) desiccated layer (Figure 12a) than for Section 2 (e.g. 1m) shown in Figure 12b. This fissuring depth could indicate that the zone of elevated resistivity shown in Figure 13b could be fissuring affected by resistivity homogenisation due to relatively large electrode spacing (Rey et al., 2006; Rey and Jongmans, 2007). These fissure depths are within the range observed by Dyer et al. (2009).

## 4.2 3-D surveys

### 4.2.1 Winter surveys

Figure 14 shows the 3-D surveys completed in March 2011. The results of the largest scale survey taken with 1m electrode spacing show a model with relatively low resistivity, with values falling below 50 ohm-m. An elevated region of resistivity of approximately 30 to 40 ohm-m occurring close to the embankment crest can be observed on both landward and estuary slopes, surrounded by regions of lower resistivity (5 to 20 ohm-m). This survey can be compared with the topographical model shown in Figure 8b. It was found that there was a 20% increase in resistivity above the input resistivity value (20 ohm-m). The model obtained with a smaller electrode spacing of 0.5m for the same section (shown in Figure 14b) confirms that this increase of resistivity is more related to fissuring rather than topography effect (Figure 14c and Figure 15).

The results show that fissures on an embankment can be imaged at a relatively large scale in 3-D which can provide important spatial information about the distribution of defects on an embankment. The zone of elevated resistivity which can be considered as the result of fissuring is more extended on the landward side of the embankment. This information is important for the proper assessment of the potential breaching mechanism that could take place on the outward side of the embankment. The values of resistivity obtained for fissured soil during the winter survey are significantly lower than those observed during the summer survey and this is true even when the surveys are taken with small scale electrode spacings such as those shown in Figure 14c and 15. The resistivity survey has also imaged some of the interconnected fissures observed, but with a relatively low resistivity when compared with those obtained in the summer and in 2-D (Figure 13). This indicates that there is a seasonal change in the embankment condition which results in a different response for a survey in summer rather than winter. The seasonal response may be explained by higher degree of

soil saturation in the winter months and possible partial closing of the cracks observed at the surface.

Despite the reduced response an estimation of fissuring depth can be obtained based on the resistivity ranges shown in Figure 15. Figure 16 shows the sections of the 3-D resistivity model showing the maximum resolved fissure depth to be 0.5m close to the embankment crest. The average depth of fissuring found here is around 0.2m, which is in line with previous estimates obtained from the 2-D miniature surveys. The cross sections reveal no subsurface interconnection, which is likely the result of the low resolution of the survey.

### 4.2.2 Summer survey

Figure 17 shows the resistivity model from the 3-D survey obtained in June 2011; the survey was completed with parallel lines of electrodes placed across the embankment from landward to estuary slope in the x-direction (Figure 17). Patches of high resistivity were observed on both slopes of the embankment. The patches extend for 6m in the y-direction on the landward slope and 10m on the estuary outward slope. Such anomalies indicate large, continuous, interconnected fissures similar to those shown in Figure 13. The resistivity patterns obtained for the slopes during this embankment survey could be compared with those obtained from the forward model with 0.5m electrode spacing (Figure 4 a to c). The embankment section imaged with this survey shows an elevated surface layer with approximately 1m thickness, underlain by a lower resistivity layer of approximately 20 ohm-m. This indicates that the soil was highly desiccated in the summer months, though the core of the embankment was largely unaffected as the resistivity values are similar to those obtained for the 2-D surveys taken on the crest, as shown in Figure 11.

A cross section of the embankment shown in Figure 17c and d shows the maximum fissuring depth of about 1m. The fissuring depth is greatest at the intersection between embankment slope and crest. This observation is similar to the results from the forward modelling discussed earlier in Section 2.1. This indicates that the fissuring depths obtained in the field

are consistent with the forward model and represent well the true fissuring found on the embankment (Dyer et al., 2009).

### 4.2.3 Significance of results

The study has produced an invaluable insight into the use of ERT in applications related to desiccation cracking in soils, benefiting both geophysical practitioners and geotechnical engineers. It is well known that vertical and horizontal fissuring beneath the surface of the soil can create an ideal preferential flow path for water (e.g. Armstrong et al., 1994; Flurry et al., 1994; Omidi et al. 1996; Drumm et al., 1997; Rounsevell et al., 1999). Thus, it is important for engineers to have a tool that will be capable of detecting the extent of desiccation cracks, especially those forming in vital infrastructure (i.e. embankments, dams and clay liners).

It is considered that ERT can be used in the future as a complementary method in conjunction with traditional visual surveys, to allow fissuring to be detected and imaged, particularly where dense vegetation obscures the soil surface. The 3-D survey presented in Figure 17 shows that fissures are prevalent on the landward face of the embankment where the vegetation is rarely trimmed, and as a result is generally denser than on the outward face (e.g. river side). Hence, it will have more effect on the hydrology of the near-surface soil (Glendinning et al., 2009). It is the most critical side of the embankment if overtopping would occur. The estuarine side of the embankment will experience more wetting at high tides, which will result in a less desiccated section and subsequently less cracking.

From an applied geophysical perspective, the use of both large and small scale arrays in the field is important. From a practical viewpoint it is necessary to perform surveys on both slopes and crest in order to gain a complete picture of the fissuring, or any other defects. In addition it would be prudent to complete such surveys in 3-D to ensure that the distribution of any defects along the embankment length can also be observed.

The practical applications of miniature surveys such as those shown in Figure 13 and small scale surveys as shown in Figure 14d with regard to a large structure such as a flood embankment are likely to be confined to situations where a large amount of detail is required. This does not mean however that such detailed surveys are completely impractical, as it is possible to imagine situations where detailed analysis of potential flow paths is needed.

# 5 Conclusions

The use of Electrical Resistivity tomography for the detection and mapping of desiccation cracks in a flood embankment has been tested in the field in both 2-D and 3-D and compared with the results from forward modelling The results show that ERT can be used to image fissures on the embankment, with high resolution 2-D surveys showing the existence of possible subsurface interconnection between cracks and 3-D surveys mapping and characterising interconnected fissures on the embankment surface. Large scale surveys with 1m electrode spacing appear to be useful in detecting zones of fissuring, though individual cracks cannot be identified and showed only the extent of desiccation. 3-D surveys taken across the embankment provided an overview of fissuring on an embankment section which also indicated differences in fissuring between the landward and outward slopes.

As a general consideration the miniature array used in 2-D provided a far greater level of resolution than the larger array with 1m electrode spacing. The same conclusions can be drawn from the smaller scale 3-D arrays (with 0.5 and 0.2m electrode spacing). The 2-D miniature surveys provided a detailed investigation into the subsurface but only over a short section of less than 5m and the 3-D small scale surveys provided reasonably detailed information about the surface fissuring patterns but only over a small area.

The effect of topography has been investigated and found to have a limited influence on the resistivity model obtained from inversion. The two surveys carried out in summer and winter months revealed an apparent drop in the resistivity values associated with fissures. This

indicates that the best results can be obtained in the summer where cracks are larger and provide a better contrast with the intact soil.

An analysis of the results indicated that the surveyed embankment had large cracks on both the landward and outward slopes, with those on landward side largely obscured by dense vegetation which prevented an accurate visual diagnosis of the slope condition.

The size of the investigated section should determine the choice of the array to be used. The high resolution miniature arrays should be used as complementary tool to the large scale surveys.

## 6 Acknowledgments

The authors would like to thank the Royal Society (Grant: RG110069) and the EPSRC (grant: EP/P505127/1) for their support towards the funding for this research. The third author would like to acknowledge the financial support provided by the EC funded project RISMAC (Grant agreement: PIOF-GA-2009-254794).

## References


Abu-Hassanein, Z.C, Benson, C. H., Blotz, L. R., 1996. Electrical resistivity of compacted clays. J. Geotech. Eng., ASCE, 122 (5), 397-406.

Albright, W.H., Benson, C.H., Gee, G.W., Abichou, T., McDonald, E.V., Tyler, S.W., Rock, S.A., 2006. Field performance of a compacted clay landfill final cover at a humid site. J. Geotech. Geoenviron. Eng.132(11), 1393–1403.

Armstrong, A.C., Matthews, A.M., Portwood, A.M., Addiscott, T.M., Leeds-Harrison, P.B., 1994. Modelling the effects of climate change on the hydrology and water quality of structured soils. Soil Responses to Climate Change. NATO ASI Series 23 [Rounsevell, M.D.A. and P.J. Loveland (eds.)]. Springer-Verlag, Heidelberg, Germany, 113-136.

BSI, 1996. BS 1377-2: Methods of test for soils for civil engineering purposes. Part 2: Classification tests. British Standards Institution, Milton Keynes.

Cho, I.-K., Kim, J.-H., Chung, S.-H., Suh, J.-H., 2002. Negative apparent resistivity in resistivity method. Geophys. Explor. 5, 199–205.

Cooling, L. F., Marsland, A., 1954. Soil mechanics studies of failures in the sea defence banks of Essex and Kent. Proc. ICE. - North Sea Floods 31 January/1 February 1953. 58-73.

Drumm, E., Boles, D., Wilson, G., 1997. Desiccation cracks result in preferential flow. Geotech. News, 15(2), 22–25.

Dyer, M., Utili, S., Zielinski, M., 2009. Field survey of desiccation fissuring of flood embankments. Proc. Inst. Civ. Eng. - Water Man. WM3, 221-232.

Flurry, M., Fluhler, H., Jury, W.A., Leuenberger, J., 1994. Susceptibility of soils to preferential flow of water: A Field Study. Water Resur. Res. 30(7), 1945-1954.

Glendinning, S., Loveridge, F., Starr-Keddle, R.E., Bransby, M.F., Hughes, P.N., 2009. Role of vegetation in sustainability of infrastructure slopes. Proc. Inst. Civ. Eng. – Eng. Sust. ES2, 101-110.

Janssen, M., Lennartz, B., Wöhling ,T., 2010. Percolation losses in paddy fields with a dynamic soil structure: model development and applications. Hydrol. Process. 24(7), 813-824.

Jones, G., Zielinski. M., Sentenac, P., 2012. Mapping desiccation fissures using 3-D electrical resistivity tomography. J. Appl. Geophys. 84, 39-51.

Johansson, S., Dahlin, T., 1996. Seepage monitoring in an earth embankment dam by repeated resistivity measurements, Eur. J. Eng. Env. Geophys., 1(3), 229-247.

Konrad, R., Ayad, J.M., 1997. Dessication of a sensitive clay: field experimental observations. Can. Geotech. J. 34, 929–942.

Keller, G.V., Frischknecht, F.C., 1966. Electrical methods in geophysical prospecting. Pergamon Press.

Kleppe, J.H., Olson, R.E., 1985. Desiccation cracking of soil barriers. In Johnson, A.I. Frobel, R.K., Calalli, N.J., & Petterson, C.B. (eds.) Hydraulic Barriers in Soil and Rock, ASTM STP 874, 263-275.

Kuras, O., Pritchard, J. D., Meldrum, P. I., Chambers, J. E., Wilkinson, P. B., Ogilvy, R. D , Wealthall, G. P., 2009. Monitoring hydraulic processes with automated time-Lapse Electrical Resistivity Tomography (ALERT). Comptes Rendus Geoscience - Special Issue on Hydrogeophysics. 341, 868–885.

La Breque, D., Heath, G., Sharpe, R., Versteeg, R., 2004. Autonomous monitoring of fluid movement using 3-D Electrical Resistivity Tomography. J. Env. Eng. Geophys. 9, 167-176.

Ling, C., Zhou, Q., Yuwei, X., Zhang, Y., Li, R., ,Liu, J. 2013. Application of electrical resistivity tomography to evaluate the variation in moisture content of waste during 2 months of degradation. J. Env. Earth Sci. 68, 57-67.

Liu, C. W., Cheng, S. W., Yu, W. S., Chen, S. K., 2003. Water infiltration rate in cracked paddy soil. Geoderma. 117, 169–181.

Loke, M. H., Barker, R. D., 1996. Rapid least-sqaures inversion of apparent resistivity resistivity sections by a quasi-Newton method. Geophys. Prosp. 44, 131-152.

Loke, H. M., 2014, Tutorial : 2-D and 3-D electrical imaging surveys. Retrieved March 30th, 2014, Geotomo: http://www.geoelectrical.com.

Marsland, A., 1957. The design and construction of earthen food banks. J. Inst. Water Eng.. 11(3), 236-258.

Marsland, A. 1968. The shrinkage and fissuring of clay in flood banks. Note No. IN 39/68, Building Research Station

Marsland, A., Cooling. L. F., 1958. Tests on full scale clay flood bank to study seepage and the effects of overtopping. Watford: Intern. Rep. No. C562, Building Res. Stat. (1958)

Met Office, 2011a. Climate: observations, projections and impacts. Report, Met Office UK.

Met Office, 2011b. Weather station data – Keyingham, East Riding of Yorkshire, UK.

Omidi, G.H., Thomas, J.C. Brown, K.W., 1996. Effect of desiccation cracking on the hydraulic conductivity of a compacted clay liner. Water, Air and Soil Poll. 89(1-2), 91-103.

Pardaens, A.K., Lowe, J.A., Brown, S., Nicholls, R.J., de Gusmão, D., 2011. Sea-level rise and impacts projections under a future scenario with large greenhouse gas emission reductions. Geophys. Res. Letters, 38(12),

Pellicer, X., M., Zarroca, M., Gibson., P., 2012. Time-lapse resistivity analysis of Quaternary sediments in the Midlands of Ireland. J. Appl. Geophys. 82, 46-58.

Rey, E., Jongmans, D., Gotteland, P., Garambois, S., 2006. Characterisation of soils with stony inclusions using geoelectrical measurements. J. Appl. Geophys. 58, 188-201.

Rey, E., Jongmans, D., 2007. A 2D numerical study of the effect of particle shape and orientation on resistivity in shallow formations. Geophys. 72(1), 9-17.

Reynolds, J.M., 1997. An introduction to applied and environmental geophysics. John Wiley and Sons, Chichester.

Rhoades, J.D., Manteghi, N.A., Shouse, P.J., Alves, W.J., 1989. Soil electrical conductivity and soil salinity: new formulations and calibrations. Soil Sci. Soc. Am. J. 53, 433-439.

Rounsevell, M.D.A., Evans, S.P., Bullock, P., 1999. Climate change and agricultural soils: Impacts and adaptation. Climatic Change, 43(4), 683-709.

Rucker, D., McNeill, M., Schindler, A., Noonan, G., 2009. Monitoring of a secondary recovery application of leachate injection into a heap. Hydrometallurgy. 99, 238–248.

Samouëlian, A., Cousin, I., Richard, G., Tabbagh, A., Braund, A., 2003. Electrical resistivity imaging for detecting soil cracking at the centimetric scale. Soil Sci. Soc. Am. J. 67(5), 1319-1326.

Samouëlian, A., Richard, G., Cousin, I., Guerin, R., Braund, A., Tabbagh, A. 2004. Three-dimensional crack monitoring by electrical resistivity measurement. Eur. J. Soil Sci. 55(4), 751-762.

Sanchez, M., Atique, A., Kim, S., Romero, E., Zielinski, M., 2013. Exploring desiccation cracks in soils using a 2D profile laser device. Acta Geotech. 8(6), 583–596.

Sentenac, P., Zielinski, M., 2009. Clay fine Fissuring using miniature geoelectrical resistivity arrays. J. Env. Earth Sci. 59 (1), 205-214.

Sentenac, P., Jones, G., Zielinski, M., Tarantino, A., 2012. An approach for the geophysical assessment of fissuring of estuary and river embankments: validation against two case studies in England and Scotland. J. Env. Earth Sci. 69(6), 1939-1949.

Shin, H., Santamarina, J., 2011. Desiccation cracks in saturated fine-grained soils: particle-level phenomena and effective-stress analysis. Géotechnique. 61(11), 961–972.

Sjödahl, P., Dahlin, T., Johansson, S. Loke, M.H., 2008. Resistivity monitoring for leakage and internal erosion detection at Hällby embankment dam. J. App. Geophys. 65, 155-164.

Smethurst, J.A., Clarke, D., Powrie, W., 2006. Seasonal changes in pore water pressure in a grass-covered cut slope in London Clay. Géotechnique. 56 (8), 523–537.

Southen, J.M., Rowe, R.K., 2005. Laboratory investigation of geosynthetic clay liner desiccation in a composite liner subjected to thermal gradients. J. Geotech. Geoenviron. Eng. 131(7), 925–935.

Style, R.W., Peppin, S.S.L., Cocks, A.C.F., 2010. Mud peeling and horizontal crack formation in drying clays. Res. Rep. 10/44, Oxford Centre for Collaborative Applied Mathematics.

Utili, S., 2012. Investigation by limit analysis on the stability of slopes with cracks. Géotechnique. 63(2), 140-154.

Van Vuuren, D., Isacc, M., Kundzewicz, Z., Arnell, N., Barker, T., Criqui, P., Berkhout, F., Hilderink, H., Hinkel, J., Hof, A., Kitous, A., Kram, T., Mechler, R. & Scrieciu, S. 2011. The use of scenarios as the basis for combined assessment of climate change mitigation and adaptation. Glob. Environ. Change. 21, 575-591.

Wilkinson, P. B., Chambers, J. E., Lelliot, M., Wealthall. G. P., Ogilvy, R.D., 2008. Extreme sensitivity of crosshole Electrical Resistivity Tomography measurements to geometric errors. Geophys. J. Int. 173, 49-62.

Wilkinson, P. B., Chambers, J. E., Meldrum, P. I., Gunn, D. A., Ogilvy, R. D., Kuras, O., 2010. Predicting the movements of permanently installed electrodes on an active landslide using time-lapse geoelectrical resistivity data only. Geophys. J. Int. 183, 543-556

Wilkinson, P. B., Chambers, J. E., Kuras, O., Meldrum, P. I., Gunn, D., 2011. Long-term time-lapse geoelectrical monitoring. First Break. 29, 77-84.

Zha, F., Liu, S., Du, Y., Cui, K., Xu, L., 2010. Characterization of compacted loess by Electrical Resistivity method. Soil Behavior and Geo-micromechanics: Proc. Sessions of GeoShanghai 2010, June 3-5, 2010, Shanghai, China, 68-73.

Zielinski, M., 2009. Influence of desiccation fissuring on the stability of flood embankments. PhD Thesis, University of Strathclyde, Department of Civil and Environmental Engineering, Glasgow, UK.

Zielinski, M.**,** Sanchez, M., Romero, E., Sentenac, P., (2011), Assessment of water retention behaviour in compacted fills. Compacted Fills: Assessment, Behaviour, Design and Construction. Proc. Inst. Civil Eng. - Geotech. Eng. Themed Issue 2011, 139-148.

## Figures

Figure 1. Exposed fissures through trenching on the disused Thorngumbald embankment (after Dyer et al. 2009).

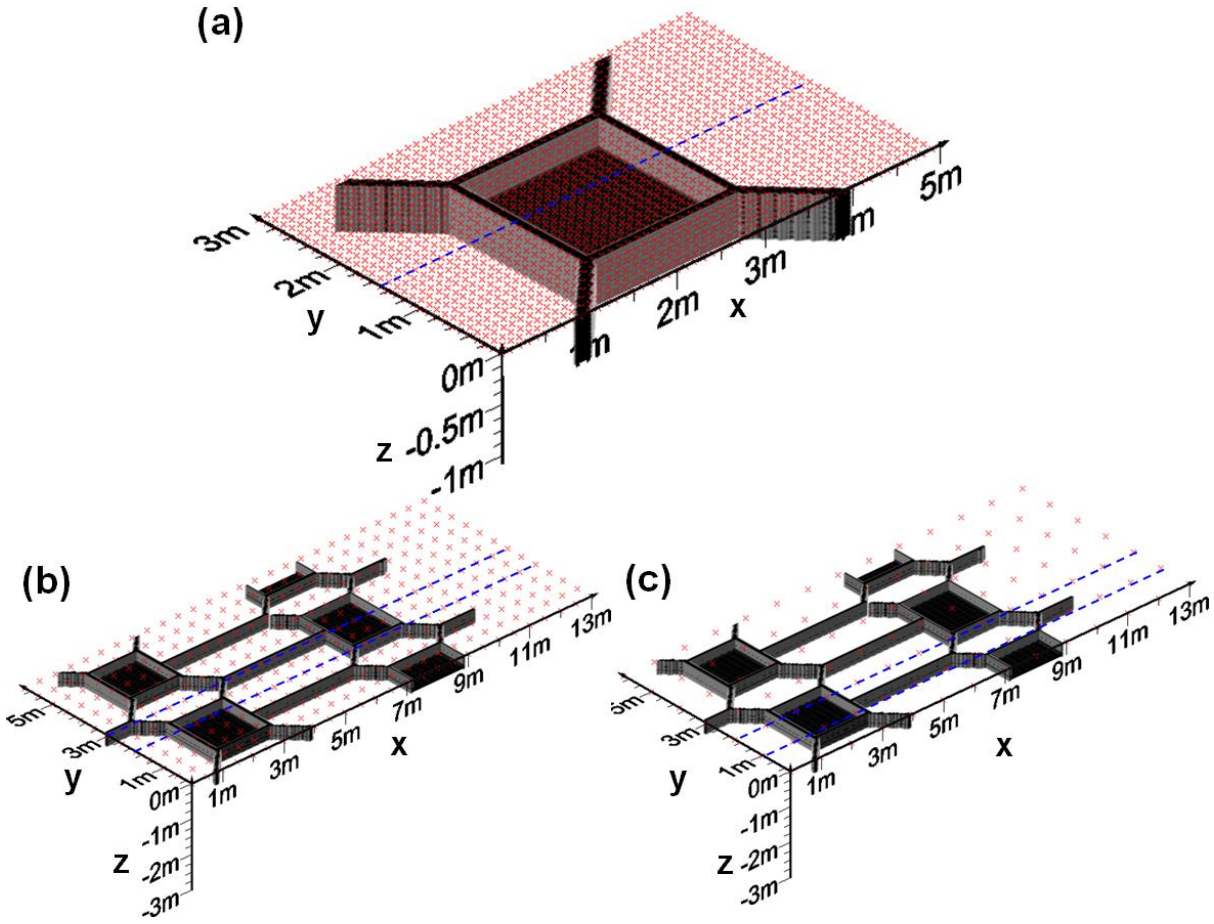


Figure 2. Fissure network input to forward models with positions of resistivity models and electrode positions indicated (a) small scale model, (b) large scale model with 0.5m electrode spacing and (c) large scale model with 1m electrode spacing.

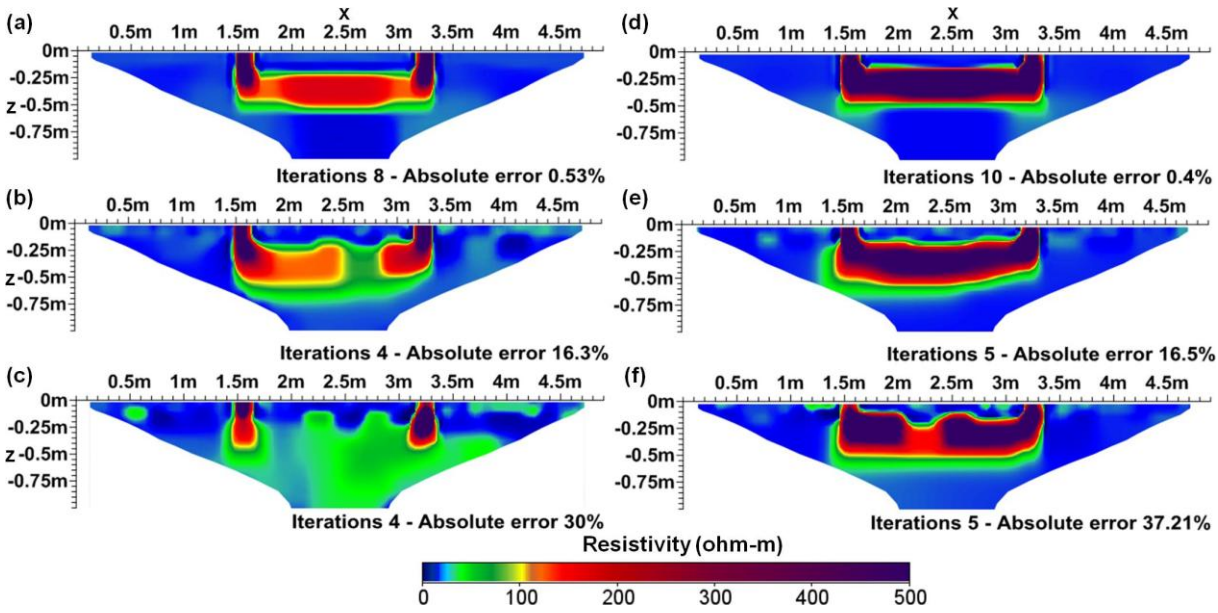


Figure 3. 2-D resistivity models obtained from inversion of data at 1.5m in the y-direction: models displayed show resistivity model for fissures of 0.5m, with (a) 0%, (b) 20% and (c) 40% added noise; and fissures of 1m depth with (d) 0%, (e) 20% and (f) 40% added noise.

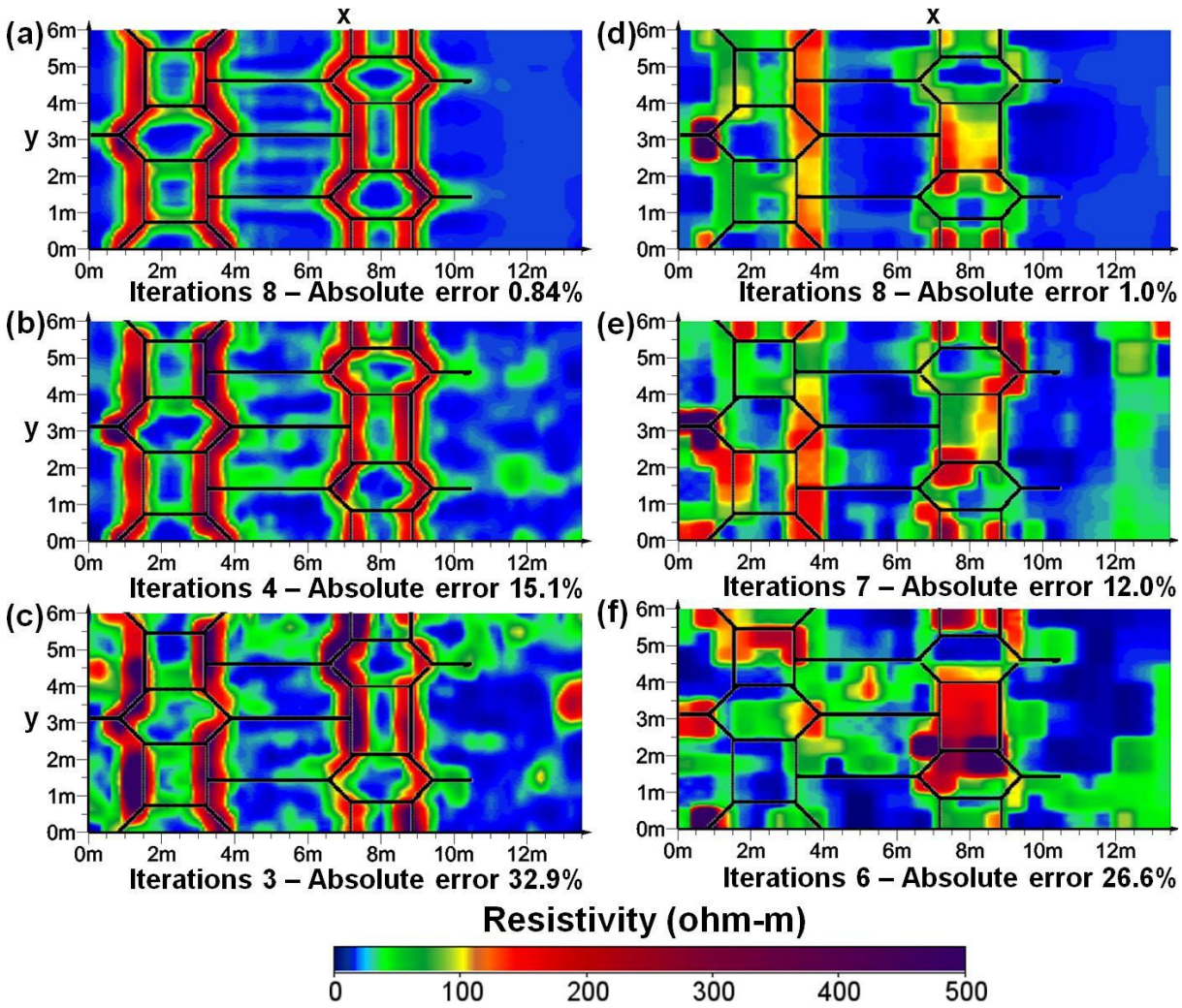


Figure 4. Surface resistivity models obtained for the large scale model with 1m fissuring depth. Inversions with electrode spacing of 0.5m are shown with noise levels of (a) 0%, (b) 20% and (c) 40% respectively and inversions with 1m electrode spacing are shown with (d) 0%, (e) 20% and (f) 40%.

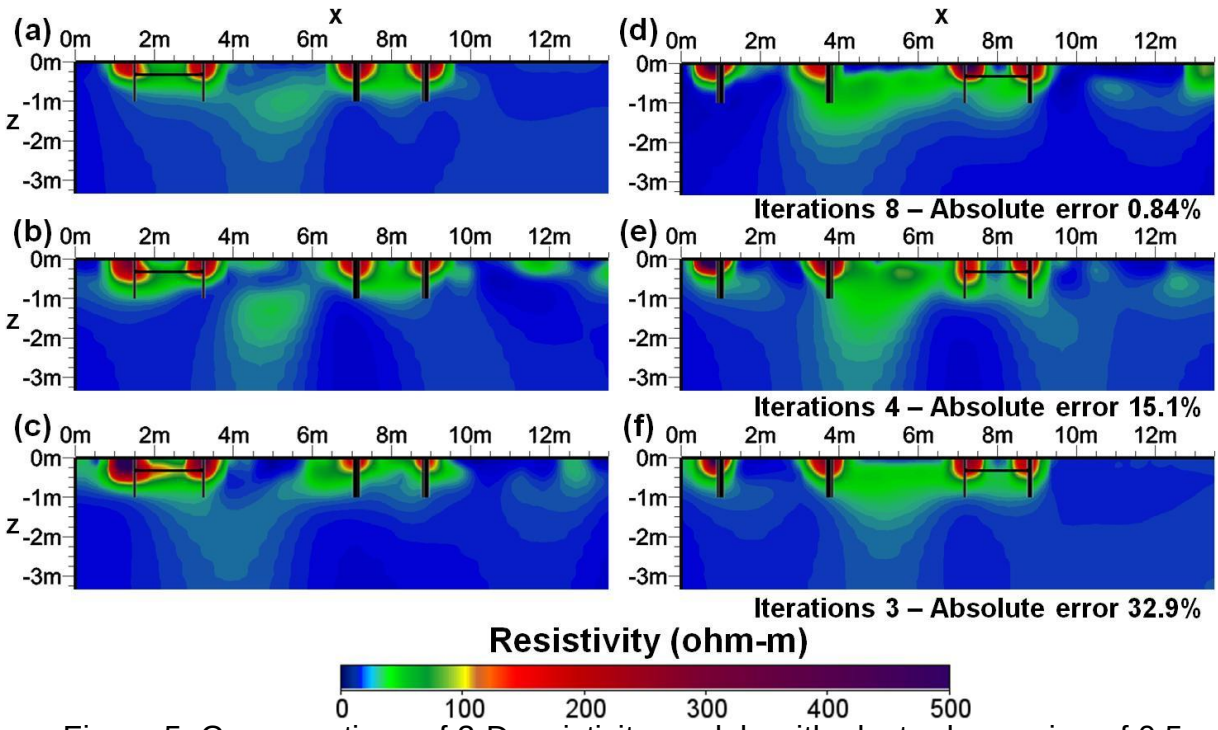


Figure 5. Cross sections of 3-D resistivity models with electrode spacing of 0.5m obtained from inversion of large resistivity model with fissuring of 1m depth, Cross sections taken in the y-direction: at 2m, with (a) 0%, (b) 20% and (c) 40% added noise; and 3m with (d) 0%, (e) 20% and (f) 40% added noise.

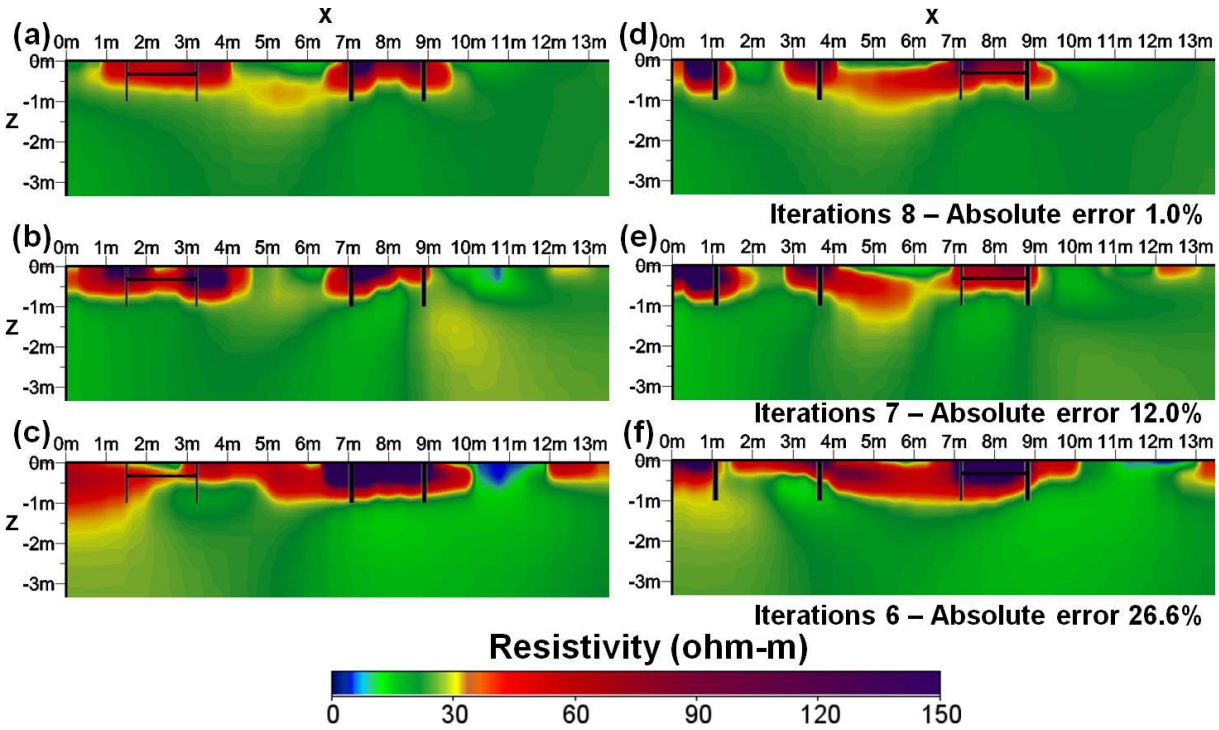


Figure 6. Cross sections of 3-D resistivity models with electrode spacing of 1m obtained from inversion of large resistivity model with fissuring of 1m depth. Cross sections taken in the y-direction: at 2m, with (a) 0%, (b) 20% and (c) 40% added noise; and 3m with (d) 0%, (e) 20% and (f) 40% added noise.

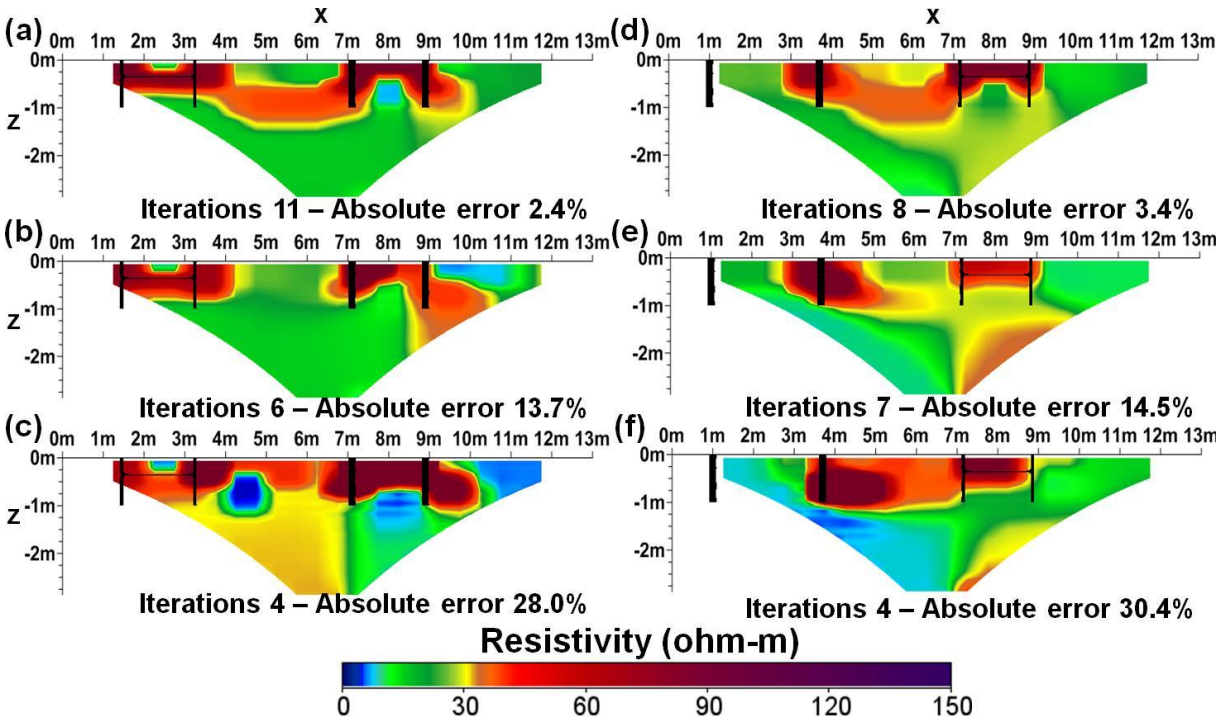


Figure 7. 2-D resistivity models obtained from inversion of large resistivity model with fissuring depth of 1m: Models shown at 2m, with (a) 0%, (b) 20% and (c) 40% added noise; and 3m with (d) 0%, (e) 20% and (f) 40% added noise.

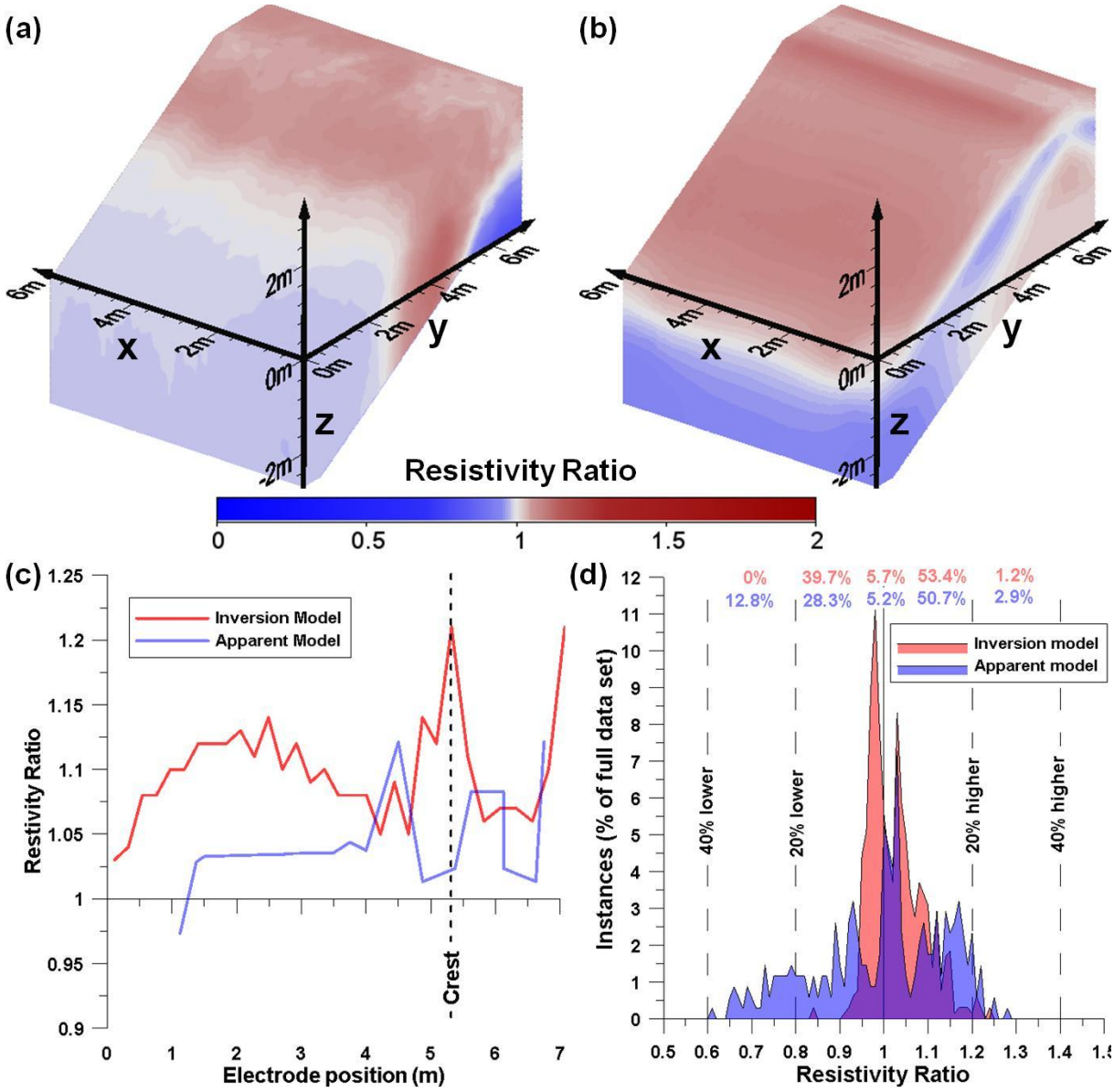


Figure 8. Results from the modelling completed to evaluate the effect of topography on the resistivity data: (a) apparent resistivity model after forward modelling, (b) inverted model, (c) resistivity ratio variation for the apparent and inverted resistivity models and (d) histogram of the resistivity data obtained from the forward model and inverted model.

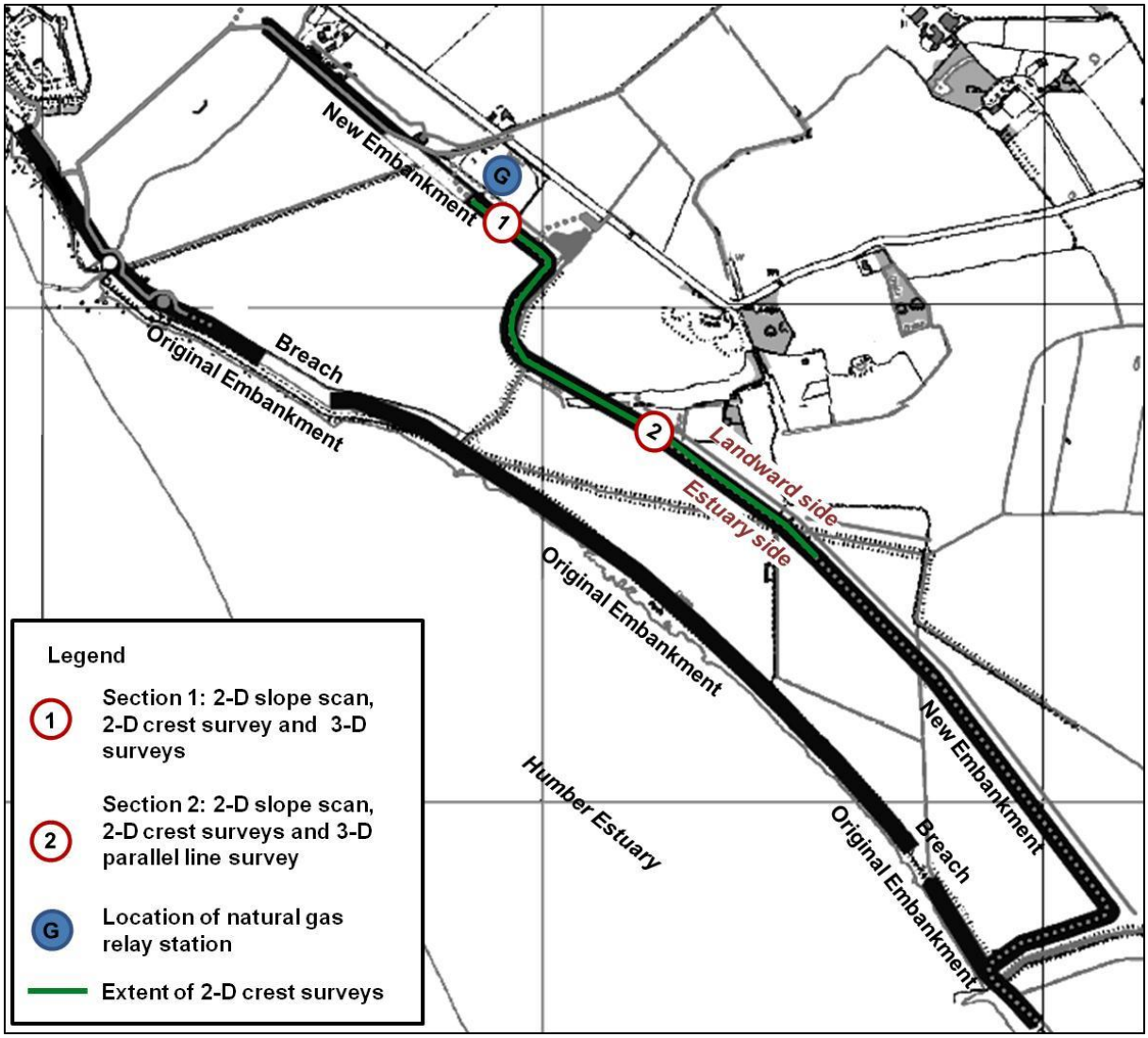


Figure 9:.Thorngumbald site plan view, indicating positions of the survey geophysical sites. © Crown copyright. All rights reserved Environment Agency. 100026380. 2012.

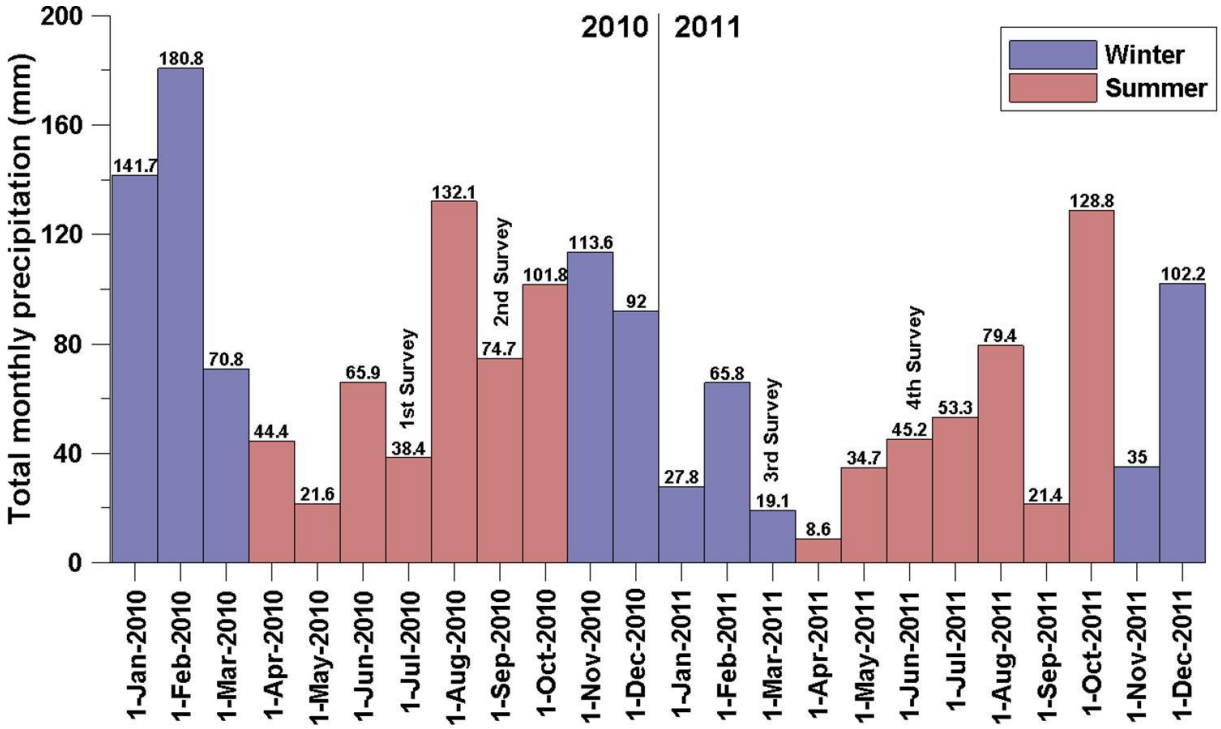


Figure 10. Total monthly precipitation close to the Paull Holme Strays site (Keyingham) showing data from 2010 to 2011, summer is based on the official British summer time from the last Sunday in March to the last Sunday in October. 

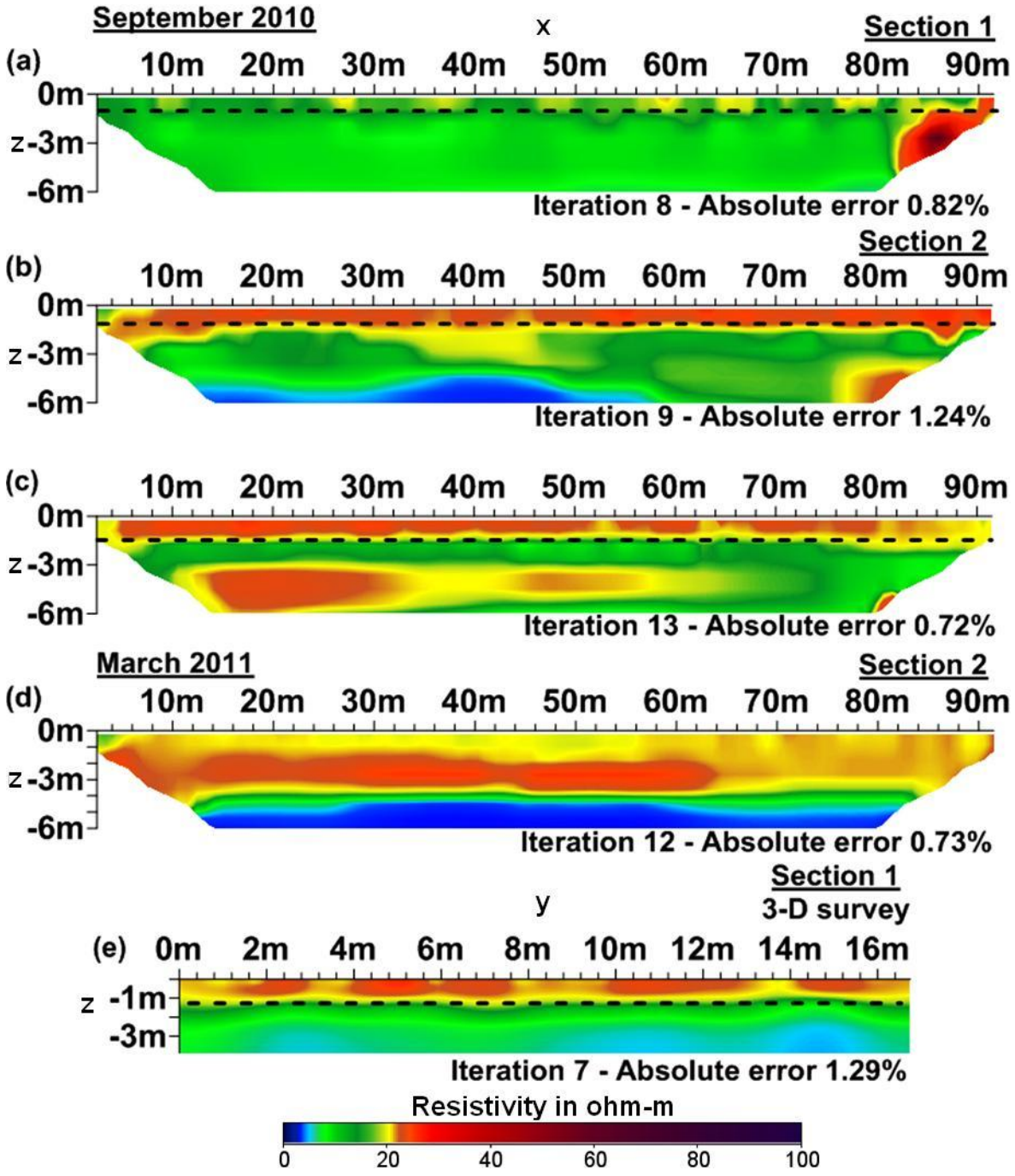


Figure 11. Surveys taken on the embankment crest with possible desiccated layer indicated by dashed line. Time of year and approximate location are also indicated.

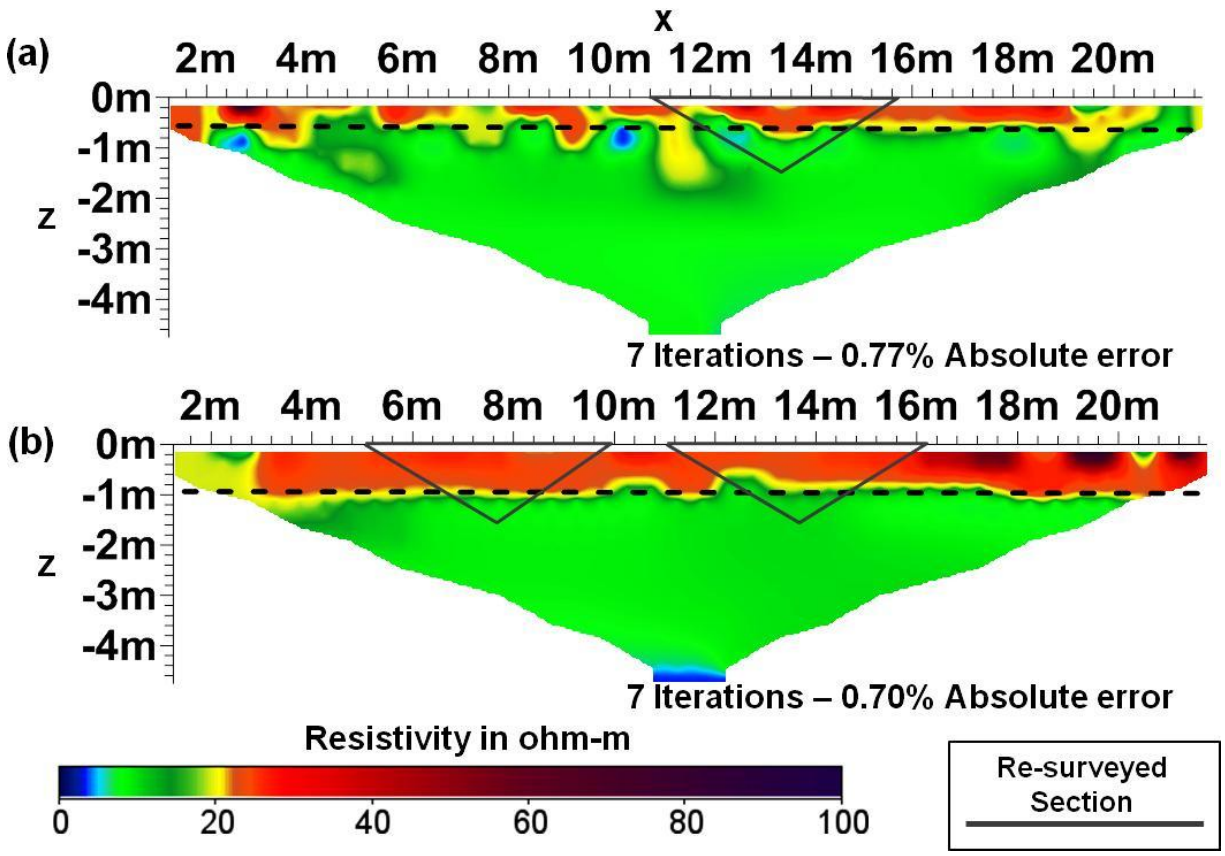


Figure 12. 2-D sections taken along the Thorngumbald embankment slope with 1m electrode spacing with section resurveyed using miniature arrays indicated (a) survey from section 1 and (b) survey from section 2. The extent of fissuring as indicated from the elevated values is shown by the dashed line, and positions of overlapping surveys are also shown. Note that the resistivity range is the same as in Figure 4.

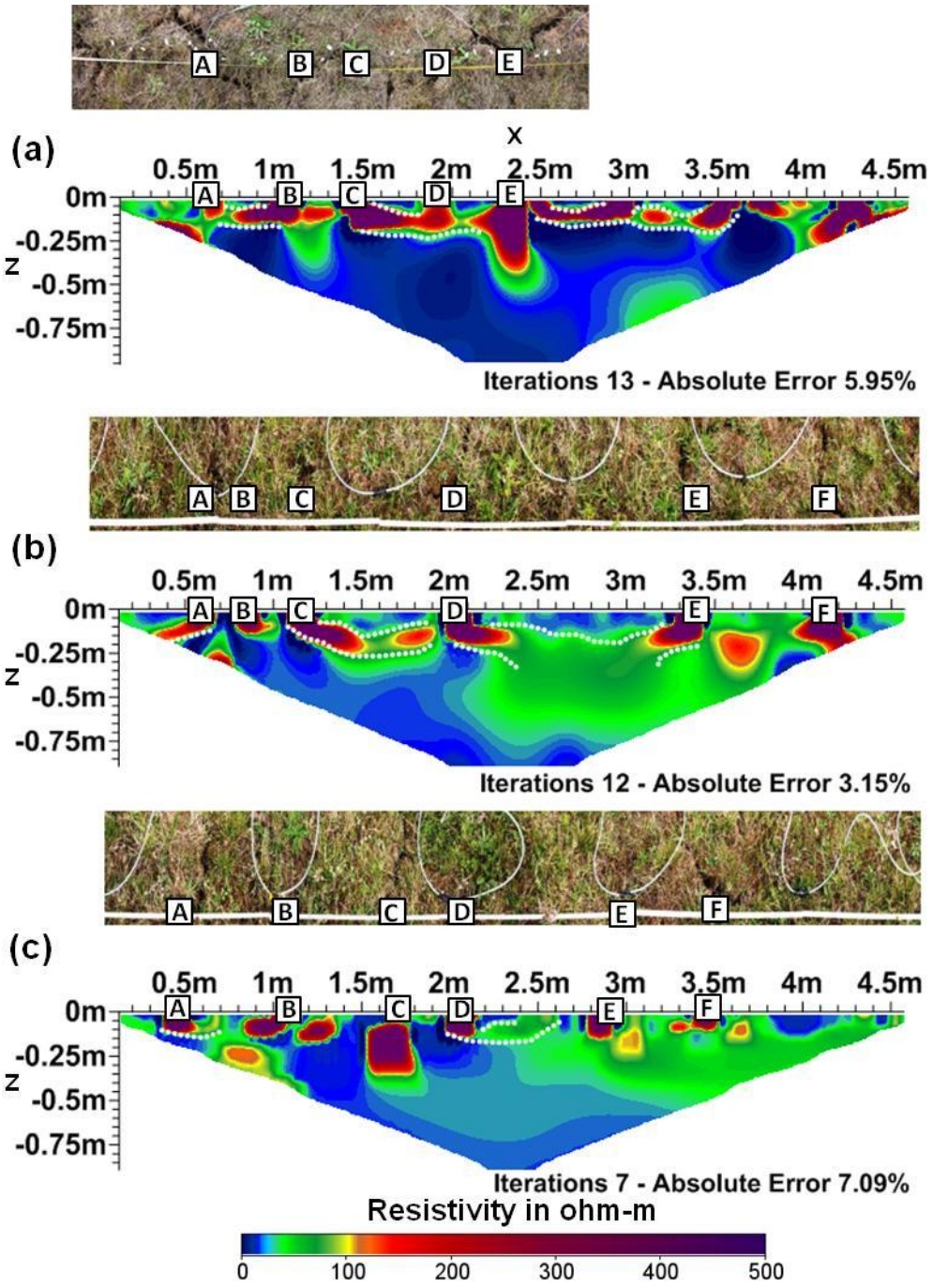


Figure 13. Miniature surveys (September 2010) with electrode spacing of 0.1m showing vertical fissuring and possible subsurface interconnection showing, (a) from section 1 and (b) and (c) from section 2.

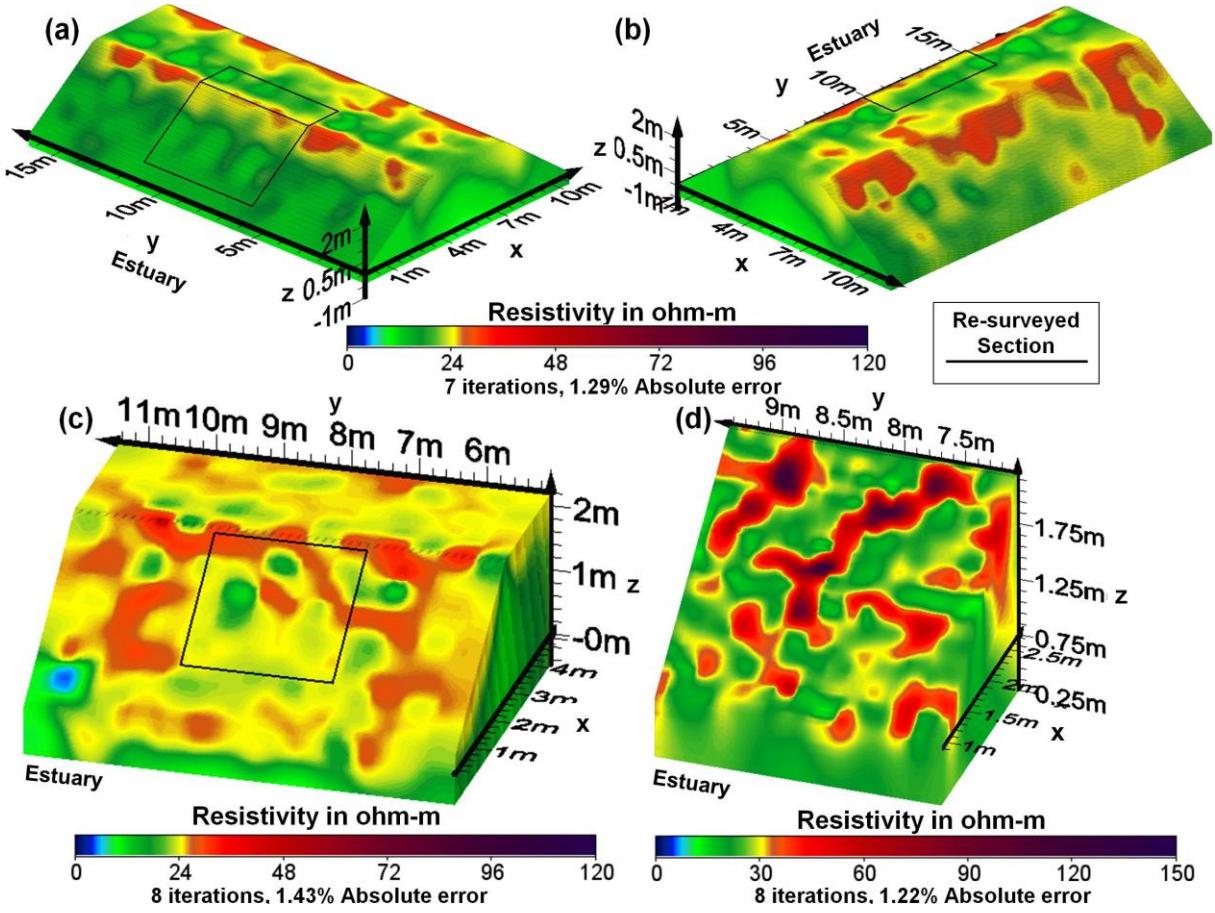


Figure 14. 3-D surveys (March 2011) showing (a) estuary facing and (b) landward facing slope of the cross embankment survey using 1m electrode spacing, (c) the overlapping crest and slope section with electrode spacing of 0.5m and (d) the small scale slope section with 0.2m electrode spacing.

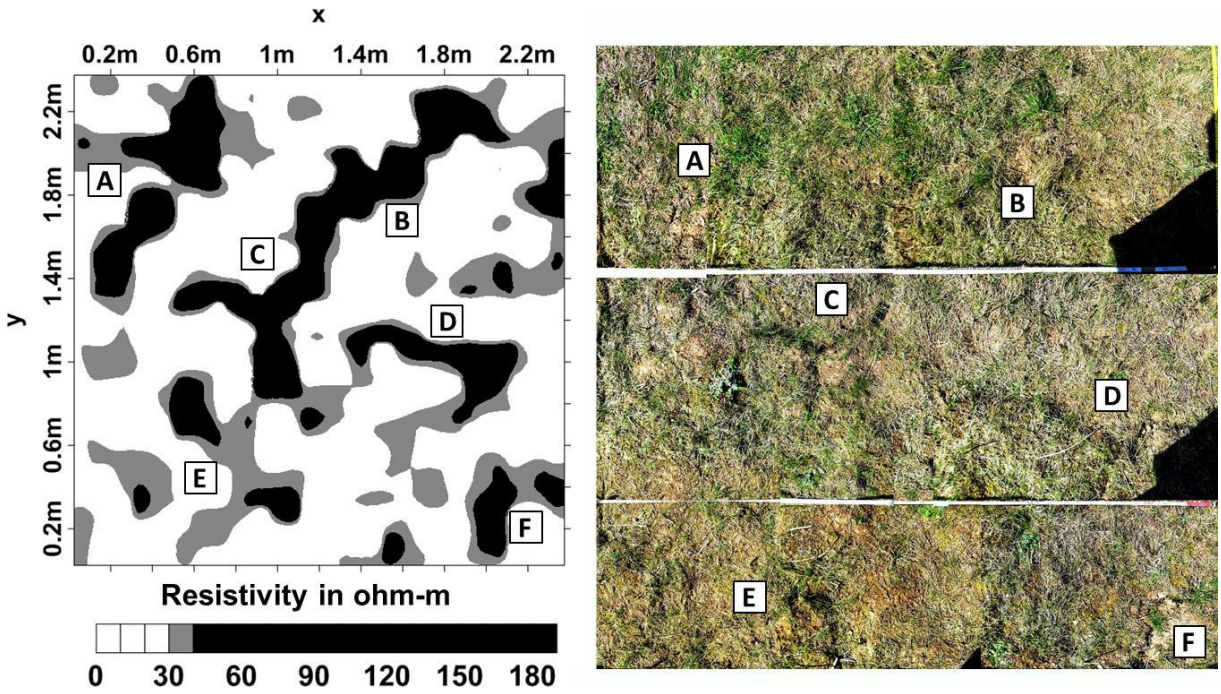


Figure 15. Small scale survey with 0.2m electrode spacing showing comparison with surface fissures

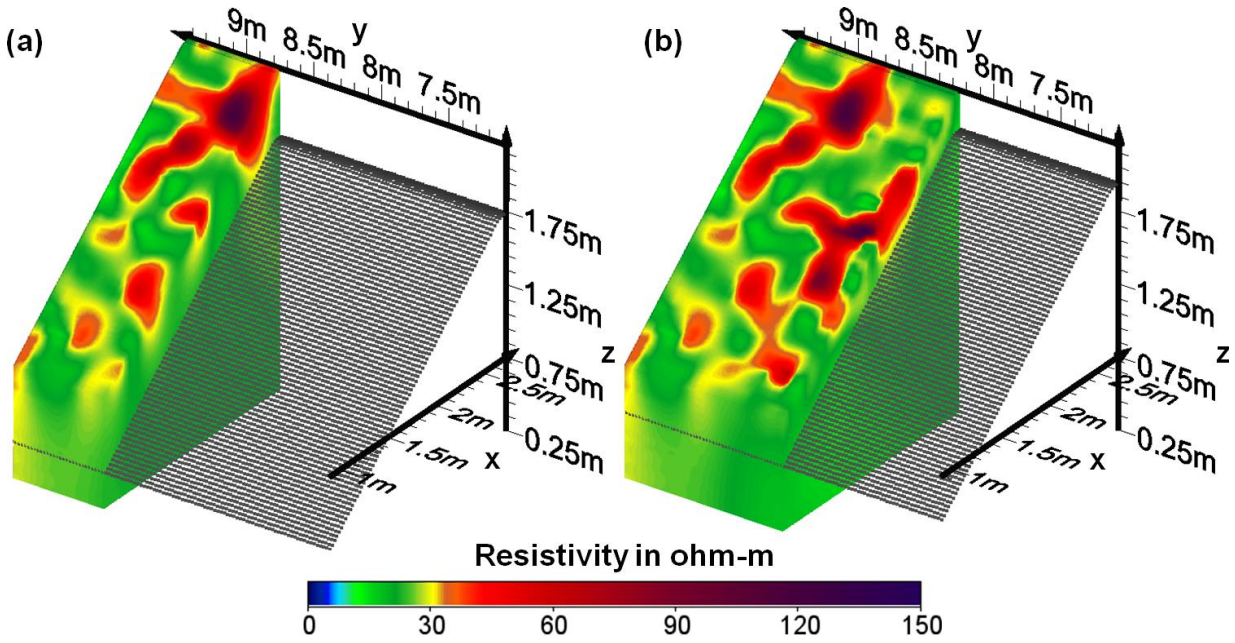


Figure 16. Slope survey with 0.2m electrode spacing with cross sections revealing subsurface fissures with (a) 0.5m depth and (b) 0.25m depth.

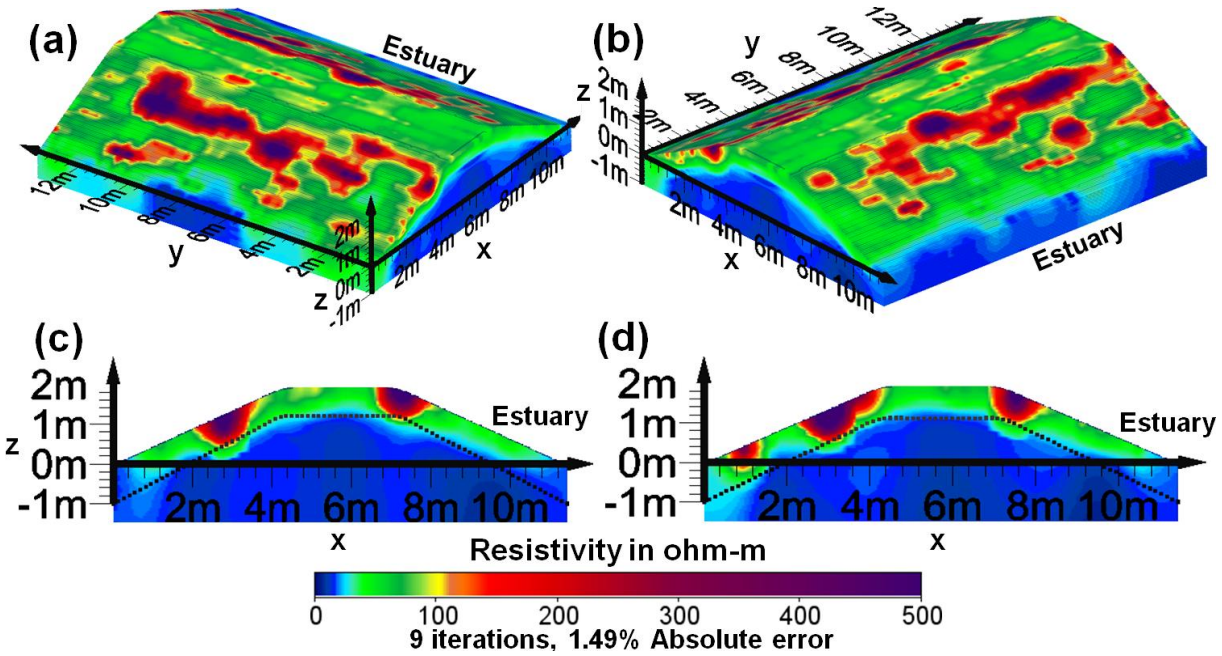


Figure 17. 3-D parallel line survey displaying the extent of fissuring on the embankment slopes showing (a) the surface networks on the landward slope, (b) the surface networks on the estuary slopes, (c) cross section at 6m in the y-direction and (d) cross section at 10m in the y-direction.